1 *Research Article.*

2 An Electromagnetically Actuated Double-Sided
3 Cell-Stretching Device for Mechanobiology Research

4 **Harshad Kamble[1], Raja Vadivelu[2], Mathew Barton[3,4], Kseniia Boriachek[2], Ahmed Munaz[1],**
5 **Sungsu Park[5], Muhammad J. A. Shiddiky[1,2], Nam-Trung Nguyen[1]***

6   [1]   QLD Micro- and Nanotechnology Centre, Nathan Campus, Griffith University, 170 Kessels Road, Brisbane,
7   QLD 4111, Australia.
8   [2]   School of Natural Sciences, Nathan Campus, Griffith University, 170 Kessels Road, Brisbane, QLD 4111,
9   Australia.
10   [3]   HealthTech-X, Menzies Health Institute Queensland, Griffith University, Gold Coast, QLD, Australia.
11   [4]   Clem Jones Centre for Neurobiology and Stem Cell Research, Griffith University, Don Young Road, Nathan
12   Qld 4111
13   [5]   School of Mechanical Engineering, Sungkyunkwan University, Suwon 16419, Korea.
14
15   *****   Correspondence: nam-trung.nguyen@griffith.edu.au; Tel.: +61-7-373-53921
16
17

18 **Abstract:** Cellular response to mechanical stimuli is an integral part of cell homeostasis. The
19 interaction of the extracellular matrix with the mechanical stress plays an important role in
20 cytoskeleton organisation and cell alignment. Insights from the response can be utilised to develop
21 cell culture methods that achieve predefined cell patterns, which are critical for tissue remodelling
22 and cell therapy. We report the working principle, design, simulation and characterisation of a
23 novel electromagnetic cell stretching platform based on the double-sided axial stretching approach.
24 The device is capable of introducing a cyclic and static strain pattern on a cell culture. The platform
25 was tested with fibroblasts. The experimental results are consistent with the previously reported
26 cytoskeleton reorganisation and cell reorientation induced by strain. The orientation of the cells is
27 highly influenced by external mechanical cues. Cells reorganise their cytoskeleton to avoid external
28 strain and to maintain intact extracellular matrix arrangements.

29 **Keywords:** Biomedical Engineering, Cell Stretching, Mechanobiology.
30

31 1. Introduction

32   Cells in a functioning multicellular system are continuously exposed to various mechanical
33 forces. The ability of the cells to recognise these mechanical stimuli and transform them into
34 chemical responses is known as a mechanotransduction.[1-3] It is well known that abnormalities in
35 mechanotransduction signalling pathways affect the cell behaviour and tissue homeostasis,
36 consequently leading to pathogenesis.[4,5]
37
38   Mechanical forces related to cyclic deformation of soft tissues are essential for the maintenance
39 of various physiological conditions of organs such as heart, blood vessels and lungs.[6] The
40 connective tissues of these organs contain a significant amount of fibroblastic cell types. The
41 mechanotransduction mechanisms in fibroblasts are crucial to modulate tissue homeostasis.[7]
42 Fibroblasts continually perceive external mechanical stimuli, which subsequently lead to the
43 production and remodelling of extracellular matrix (ECM) components. For instance, numerous
44 studies have reported that under cyclic or static strain, fibroblast cells synthesise the ECM
45 protein.[8] Fibroblasts anchor their actin cytoskeleton with ECM by linkage proteins called integrins.

46   Integrins act as mechanosensors that sense the physical forces applied onto the cell surface. The
47   ECM-integrin-cytoskeleton integration plays a vital role in the functional and structural adaptation
48   of cell in response to mechanical cues.[9] These mechanical signals are then transmitted to
49   cytoskeleton by the formation of ECM-actin cytoskeleton linkage. This complex system promotes the
50   assembly of focal adhesion, thereby induces the reconstruction of actin cytoskeleton that is necessary
51   for cell stiffening, gripping and adherence.
52
53   The cytoskeleton reorganisation exerts adaptive response in the cell under mechanical
54   stimuli.[10] This process enables cells to regulate the formation of new lamellaipodia and to adjust
55   their adhesion to resist physical deformation.[11,12] Thus, cell displacement has been observed for
56   different amplitudes, types and directions of mechanical strain. For instance, cyclic stretching at high
57   frequency aligns the cells perpendicularly to the stretching direction.[13] In contrast, static stretching
58   induces cells to align parallel to the stretching direction.[14] Hence, better understanding of the
59   cellular response of the fibroblast culture upon mechanical stimuli provides insight into examining
60   how mechanical factors alter the physiology and behaviour of the fibroblasts. Thus, various
61   techniques have been developed to introduce mechanical stimuli to the cellular microenvironment.
62   Considering the complex *in-vivo* microenvironment of the cells, the majority of the cell stretching
63   approaches has been developed as *in-vitro* platforms.[15-18]
64
65   Most cell stretching approaches include the use of tweezers or micropipettes to induce the
66   mechanical stimuli.[19-22] However, commercial cell stretching platforms such as Flexcell (Flexcell
67   International Corporation), Strex Systems for cell Stretching (STREX Inc.) and ElectroForce have
68   been recently available.[23-25] Moreover, various customised stretching platforms have been
69   reported in the last decade. The majority of these platforms utilises either electromagnetic,
70   pneumatic, piezoelectric or optical actuators to deform an elastic membrane with cell cultured on it.
71   [15,26-29] For instance, Shimizu *et al.*Shimizu, *et al.* [Bibliography] developed a microfluidic device
72   with serially connected balloons. The authors utilised a positive pressure to inflate the balloons and
73   directly induce strain onto the cells. Similarly, Kamotani *et al.* Kamotani, *et al.* [Bibliography]
74   designed a microfluidic device with a deformable membrane at the bottom and an array of piezo
75   electrically actuated pins, which were placed below a microwell plate. Each microwell was
76   independently actuated by the pin, which deforms the micro-well membrane with cells cultured on
77   it. Furthermore, Huang *et al.*Huang, *et al.* [Bibliography] designed a cell stretching platform with
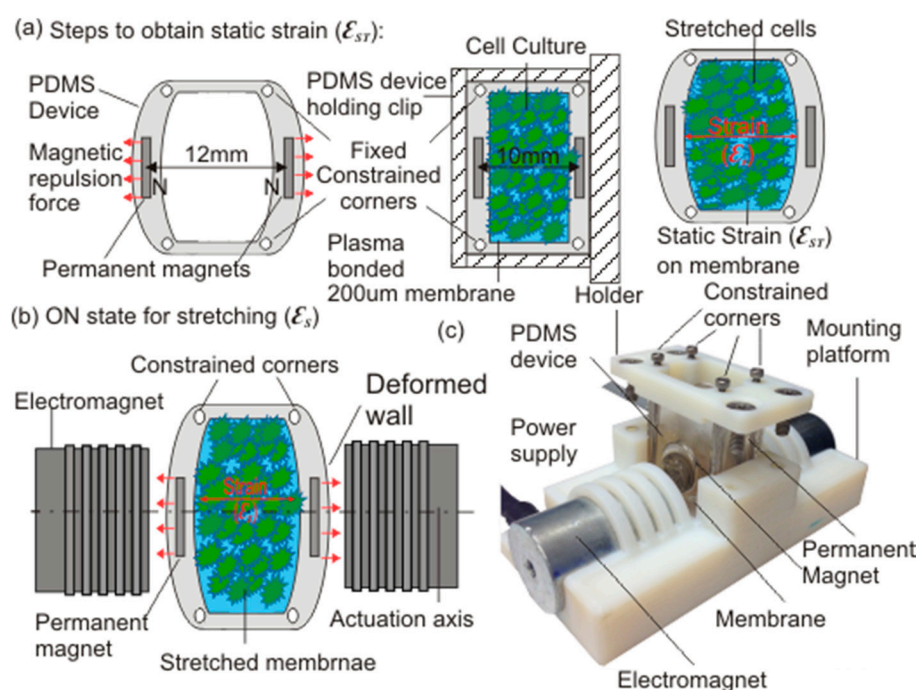

Fig. 1 Schematic illustration of the working principle: (a) Steps to obtain static strain; (b) ON state for cyclic stretching condition; (c) Actual cyclic cell stretching platform and the PDMS device.

78   indenter and utilised a servomotor to introduce strain onto the deformable membrane. In another
79   study, Sraj *et al.*Sraj, *et al.* [Bibliography] designed a microfluidic channel and utilised a single-mode
80   laser (830 nm, 200 mW) to trap and deform the cells.
81
82   Besides the above mentioned actuation approaches, electrothermal, electrostatic and
83   dielectrophoretic actuations have recently been adapted to introduce mechanical force onto the
84   cells.[34-36] All cell stretching approaches reported in the literature have their specific advantages.
85   However, very few platforms provide the main features of a robust cell stretching tool such as
86   standardised strain pattern, a wide range of imaging options and high-throughput capability. This
87   paper presents a novel cell stretching platform with a double-sided uniaxial magnetically actuated
88   stretching approach to introduce both homogeneous cyclic or static strain onto the cell culture. The
89   cell stretching platform provides homogenous and a wide range of strain values, cyclic and static
90   stretching modes, compatibility with general clinical tools and imaging options. Thus, our system is
91   suitable for long-term cell stretching studies. The present paper discusses in details the modelling,
92   fabrication and characterisation of the cell stretching platform and provides preliminary observation
93   of the response of fibroblasts under cyclic, static stretching and non-stretching conditions.

94   **2. Materials and Methods**

95   *2.1 Device design and working principle*

96   Figure 1 illustrates the schematic of the stretching platform. The platform consists of the PDMS
97   device with embedded permanent magnets, holding clip for the static strain condition and a
98   mounting stage with electromagnets for cyclic strain condition. The PDMS device has two NdFeB
99   disc magnet (15mm diameter and 2mm thickness) embedded in the front and back walls, which are 4
100 mm thick and placed 8 mm apart from each other.
101   The permanent magnets are positioned along the actuation axis, such that the north poles of
102 both magnets are facing each other to induce the repulsive force and to deform the front and back
103 walls of the PDMS device. This active magnetic repulsion was utilised to introduce the static strain
104 onto the deformable membrane.   The custom made 3D printed holding clip was used to overcome
105 the active magnetic repulsive force and to maintain the PDMS device in a predefined position. The
106 200-μm thick deformable membrane was then bonded at the bottom of the device after oxygen
107 plasma treatment. Removing the holding clip results in the desired static strain on cells cultured on
108 the deformable membrane, Fig. 1a. This simple but effective strategy allows for achieving a wide
109 range of predefined strain onto the deformable membrane, simply by controlling the initial and final
110 position of the holding clip during the bonding process of the deformable membrane and the PDMS
111 body.
112   For cyclic strain, two axially aligned electromagnet (JL Magnet) controlled by a DC power
113 supply (MK Power) was used simultaneously to externally actuate the magnets embedded in the
114 PDMS device. The mounting platform was 3D printed to introduce the necessary constraint onto the
115 PDMS device and to provide axial alignment for the permanent magnets (PMs) and electromagnets
116 (EMs). Upon actuation, the magnetic forces generated by the EMs and the PMs deform the front and
117 the back wall of the PDMS device. This force is further transferred to the deformable membrane,
118 which in turn induces a well-defined strain onto the cells cultured there, Fig.1b. Fig. 1c shows the
119 actual developed cell stretching device capable of inducing homogeneous cyclic strain onto cells
120 cultured on a deformable membrane for studying the cell behaviour.

121 *2.2 Modelling and fabrication*

122   Finite element analysis (FEA) model of the PDMS device was formulated in COMSOL
123 Multiphysics 5.2 (COMSOL, Inc.) to understand and to optimise the stretching device. We modified
124 and updated the previously reported FEA model to achieve the necessary parametric optimisation
125 of the device.[37]   The grade of the permanent magnets (PMs) was the key optimisation parameter,

126   which was taken under consideration to manipulate the active magnetic repulsive force to obtain
127   optimised static strain condition for the PDMS device without physically damaging the device.
128   To start with, a reference FEA model was formulated in COMSOL to understand the magnetic field
129   requirement. The two PMs were defined at the axial distance of 8 mm and the diameter and
130   thickness of the PMs were defined as 15 mm and 2 mm, respectively. The NdFeB material was
131   assigned for the adapted geometry and the PMs were modelled using Maxwell-Amperes law.

132                                $$\nabla \times \mathbf{H} = \mathbf{J} \; , \mathbf{B} = \nabla \times \mathbf{A} \; , \; \mathbf{J} = \sigma \, \mathbf{E} \, \mathbf{B}$$ (1)

133   where **B** is magnetic flux density in T, **E** is an electric field in V/m, A is magnetic vector and **H** is the
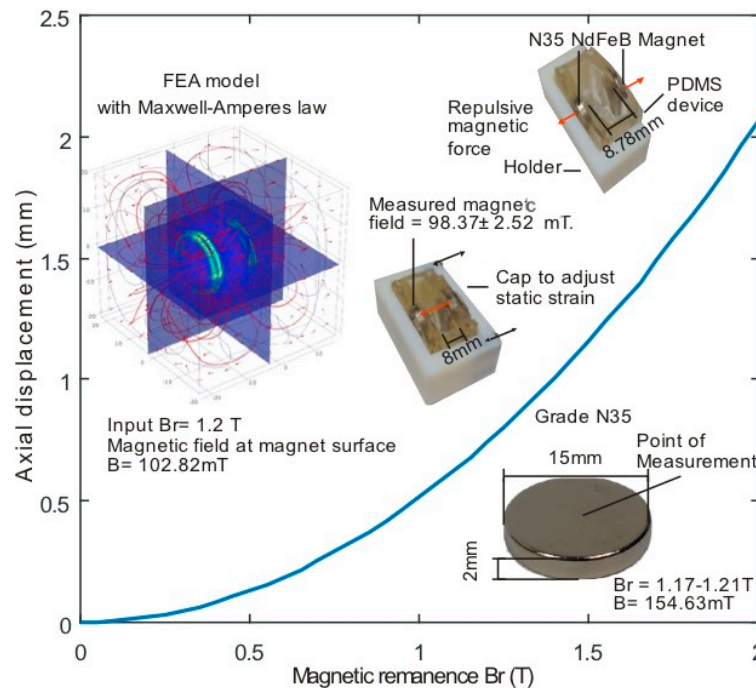134   magnetic field strength in A/m.

Fig. 2 Simulated axial displacement versus magnetic remanence. (Inset: FEA results with Br=1.2T, selected

NdFeB grade N35 magnet, PDMS device with static strain condition).

135
136   Furthermore, the optimisation was carried out by varying one parameter while maintaining the
137   other parameters constant. Maintaining the geometrical parameters constant, the magnetic
138   remanence (*Br*) of the PMs were varied over the range of 0.05T to 2T with the step of 0.05T using
139   parametric sweep function to model the variation of the NdFeB magnet grade. The inset in Fig. 2
140   shows the results for the FEA model with an input magnetic remanence (Br) of 1.2 T. In the next step,
141   to measure the corresponding deformation, the FEA model geometry of the PDMS device was built
142   with the front and back wall thickness of 4 mm, the side wall thickness of 2 mm, deformable
143   membrane thickness of 0.2 mm and axially aligned PMs with 15 mm diameter and 2 mm thickness
144   embedded into the front and back wall. The total volume of the geometry formulated in COMSOL
145   was 30x25x12 mm^3.
146   Next, the study of structural mechanics and the magnetic force was coupled in COMSOL to
147   estimate the outward force acting on the front and back walls for various values of magnetic
148   remanence. The appropriate material properties (750kPa Young's modulus and 0.49 Poisson's ratio
149   for 10:1 PDMS-cross linker mixture) were selected to match the real device. All four corners of the
150   device were fixed to maintain the necessary boundary conditions. Figure 2 shows the average
151   displacement versus the magnetic remanence of the PMs along the actuation axis. The parametric
152   optimisation suggested that an 1.2-T magnetic remanence (Grade N35) yields a magnetic flux of
153   103 mT at the surface of the PM and generated an average displacement of 0.788 mm between the

154 two embedded PMs along the actuation axis. Thus, for the static condition, the magnetic repulsion
155 facilitated a maximum static strain of 9.85% onto the membrane. Considering the experimental
156 requirement, a NdFeB magnet of grade N35 was selected for the cell stretching system.
157   The next step was the fabrication of the optimised design. The fabrication process involved the
158 fabrication of a master mould, mounting platform, and PDMS device. To start with, the aluminium
159 master mould was designed and fabricated to replicate the PDMS device with the optimised
160 geometry. The mounting platform and holding clip was designed in SolidWorks 2013 to achieve the
161 necessary constrain and axial alignments. Finally, the optimised mounting platform and holding clip
162 design was 3D printed using Eden 260V printer (Stratasys Ltd.). In the final step, the PDMS device
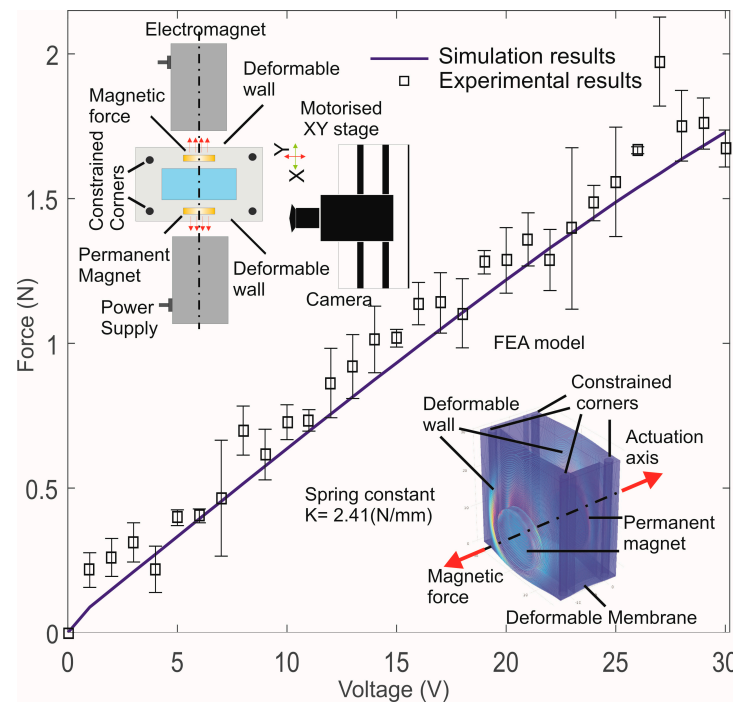163 and the deformable 200 μm membrane was fabricated.

Fig. 3 Magnetic force over the voltage range of 1- 30V (Inset: Experimental setup and FEA model for PDMS device).

164   For the fabrication of the PDMS device, 20 g of degassed mixture of PDMS and cross linker
165 (Sylgard 184 elastomer kit, Dow Corning, USA) was prepared with a volume ratio of 20:1. The
166 mixture was poured into the master mould and was again degassed for 15 minutes to remove any
167 remaining air bubbles.   The mould was then carefully closed to cure the PDMS mixture for 2 hrs at
168 80°C in a vacuum oven. Once cured, the mould was carefully opened and the PMs were placed into
169 the created cavities such that the north pole of both magnets facing each other to achieve active
170 magnetic repulsion condition. To fix the magnets in position, a small amount of PDMS-cross linker
171 mixture (10:1 volume ratio) was coated onto the PMs. The mould was then carefully closed and
172 cured for another 30 minutes at 80°C in a vacuum oven to ensure the proper placement of the PMs.
173 The cured PDMS device was then inspected and carefully removed from the mould.   Finally, the
174 PDMS device was cleaned with isopropanol and DI water. In the next step, a degassed PDMS-cross
175 linker mixture with volume ratio of 10:1 was spin coated at 4000 rpm for two minutes and cured at
176 80°C for two hours to achieve the 0.2-mm thick deformable membrane. The cured membrane was
177 inspected to confirm the uniform thickness and then cleaned with isopropanol and DI water. In the
178 last step, the PDMS device was plasma bonded with the deformable membrane and cured for one
179 hour at 80°C.
180
181
182

183   *2.3 Cell culture*

184   Fibroblast cells were cultured in DMEM/F12 (Gibco, Thermo Fisher Scientific) medium with
185   10% FBS and 1% penicillin at 37°C and 5% CO_2 in a standard incubator. To sterilise the device, the
186   device was treated with 80% ethanol and washed three times with 1X PBS followed by UV exposure
187   for 20 minutes. Before seeding the cells, the device was treated with fresh media and incubated for
188   one hour under standard condition (37°C and 5% CO_2) to further ensure its biocompatibility. For
189   seeding the device, 80% confluence was reached and the cells were harvested at the optimised
190   density of 75x10³ Cells/250 µl. In order to achieve an optimal adherence and growth of the cells onto
191   the membrane, the device was incubated at 37°C and 5% CO_2 for 24 hours before the mechanical
192   strain was applied.

193   *2.4 Application of strain on fibroblasts*

194   Two stretching modes were tested: cyclic and static axial stretching and compared to the
195   non-stretching (control) condition for this study. Cyclic stretching was applied to cells with 1.4%
196   strain at 0.01 Hz and 50% duty cycle. Under the static condition, 1.4% strain was applied to the
197   fibroblast cell culture. The strain was introduced onto the cells over 5 different time instances (0.5 hr,
198   1 hr, 2 hr, 3 hr and 4 hr) for a maximum of 4 hours. Cell characteristics such as area, aspect ratio and
199   orientation was observed after stretching and compared to the control. For the analysis, the central
200   region of the membrane was imaged with an inverted microscope (Nikon Eclipse Ts2). Biological
201   triplicates were performed.

202   *2.5 Cell fixing, immunofluorescence staining and imaging*

203   The stretched cells were fixed after stretching 4% PFA for 15 minutes followed by the three
204   10-minute washes with PBS. The deformable membranes with fixed cells were stored in the PBS
205   solution at 4°C. For actin and nuclei observation, cells were incubated with ActinGreen™ 488 and
206   NucBlue™ ReadyProbe™ Reagent (ThermoFisher Scientific) for 30 minutes followed by the three
207   post-staining washes with PBS. Images of the cell nuclei and actin fibres were finally obtained with a
208   fluorescent microscope (Olympus DX50) using 10X and 20X magnification.

209   *2.6 Image analysis*

210   For the image analysis, three seprate locations within the central region i.e. the region of
211   interests (ROI) with homogenous strain, were captured. Each image was enhanced using post
212   processing with Image J (NIH), which mainly included FFT bandpass filtering, sharpening,
213   enhancing image contrast and thresholding. For quantification, the captured cells were analysed to
214   estimate the averaged area, aspect ratio and orientation of the cells in ROI at each time instance.
215

216   **3. Results and Discussion**

217   *3.1 Force calculation*

218   For estimating the experimental magnetic force, we utilised a similar approach as reported in
219   our previous work.[38] The optimised FEA model of the PDMS device was utilised to obtain the
220   spring constant for the experimental condition. Considering the stretching condition, the magnetic
221   actuation is modelled in COMSOL by introducing an outward force onto the PMs to deform the
222   front and back walls of the PDMS device. The force was varied over the range of 0.5 N to 1 N in steps
223   of 0.5 N to observe the corresponding displacement of the PMs. Considering the material
224   properties, we assumed the Hooks law to obtain the spring constant *k* for this study:

225                               $F = -k.x,$ (2)

226   where, *k* is the spring constant in N/mm, *F* is the force in N and *x* in the displacement in mm.
227

228   The next step was to experimentally obtain the displacement of the PMs over the applied
229   voltage. Both EMs were simultaneously actuated by supplying the voltage ranging from 1 V to 30 V.
230   The corresponding displacement of the marked points on the PDMS device wall along the actuation
231   axis was recorded for each step using a digital camera (EO Edmund Optics). Furthermore, our
232   particle tracking algorithm based on digital image correlation and Matlab image processing toolbox
233   was utilised to detect and measure the displacement of the randomly marked points.[38] Finally, the
234   obtained average displacement was used to calculate the force using the spring constant of
235   2.41N/mm determined by the FEA simulation.
236   We modified and updated our previously reported FEA model to calculate the magnetic force
237   between PM and EM[37] and to validate the experimental data. We considered the symmetric nature
238   of the system and obtained the magnetic force at the PM surface along the actuation axis over the
239   voltage range of 1V - 30V.[37]   The simulation results were verified with the experimental data, Fig.
240   3. As expected, a linear force-voltage relationship can be clearly observed from Figure 3. The
241   simulation agrees well with the experimental data. The results provide an acceptable error variance
242   of 9.42% over the range of 9 V to 30 V between experimental and simulation data.

243   *3.2 Strain calculation*

244   Characterisation of strain applied to the deformable membrane was observed using both
245   experiments and simulation. For measuring the strain experimentally, the membrane deformation
246   was recorded with a digital camera (EO Edmund) over the voltage range of 1 V to 30 V. The particle
247   detection and displacement measurement algorithm based on digital image correlation and Matlab
248   image processing toolbox was further utilised to calculate the offset displacement of the marked
249   points. For reliable experimental data, the membrane of each recorded image was divided into the
250   2x5 regions. A minimum of three marked samples from central region ($M_{1,2}$, $M_{1,3}$, $M_{2,2}$, $M_{2,3}$) was
251   observed.   Finally, to warrant the repeatability of the results, three experimentally obtained results
252   were averaged to represent the displacement of the region. The inset of Fig. 4 depicts the
253   experimental setup and example of the particle detection and tracking algorithm result.
254
255   For cross validating the experimental data, we utilised a reference FEA model. The magnetic
256   force obtained from the force calculation (Section 3.1) over the voltage range of 1-30 V was used as
257   the input for the FEA model. The central region of the membrane was considered as the region of
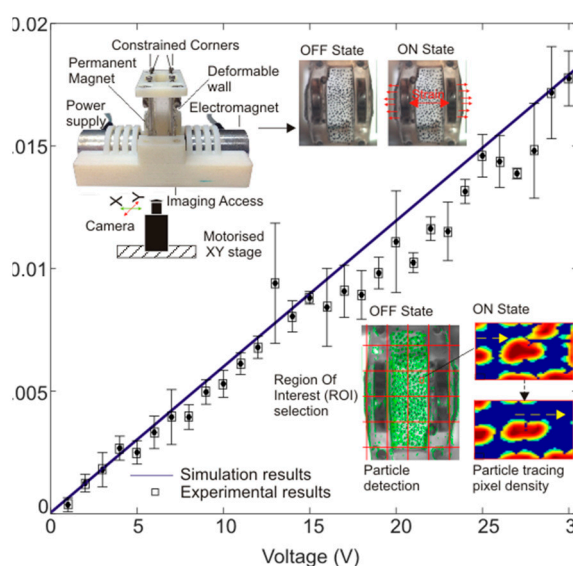258   interest (ROI).

Fig. 4 Strain on the deformable membrane over the voltage range of 1-30V. (Inset: Experimental arrangement, the membrane in ON and OFF state, an example for the particle detection and tracking.)
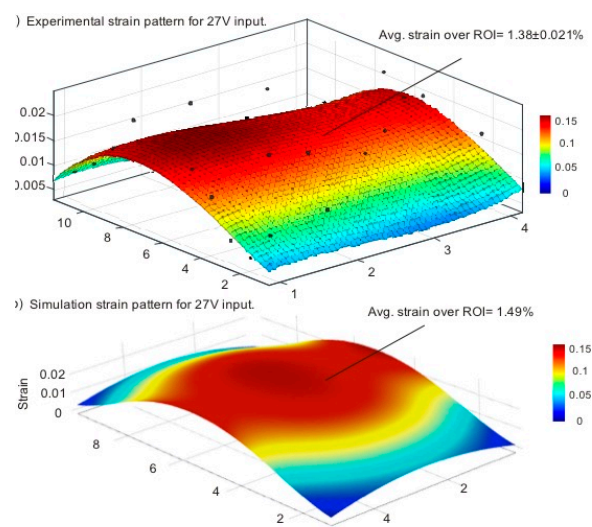

Fig. 5 Strain pattern on the membrane with a selected input of 27 V: (a) Experimental results; (b) Simulation results.

259
260   An average strain across the membrane was obtained for the operating voltage range i.e. 1 V to 30 V.
261   Figure 2 compares the average strain over the ROI from both simulation and experiments. The
262   experimental and simulation results agree well. An average error variance of 7.89% was observed
263   over the voltage range of 9 V to 30 V. Based on the strain characterisation, we selected an input
264   voltage of 27 V for both actuators, which provided an average homogeneous cyclic strain of
265   1.38±0.021% over the central region of the membrane.
266   For understanding of the membrane deformation and strain pattern with the selected input
267   voltage of 27 V, we utilised the same experimental platform and obtained the image sequence for the
268   membrane deformation. The images were analysed using the existing particle detection and tracking
269   algorithm to obtain the strain pattern over the 2x5 region matrix. A minimum of three marked points
270   from each subregion was evaluated to obtain reliable results. Finally, the average value was utilised
271   to represent the strain over each predefined subregion. Furthermore, three experiments were
272   conducted for each set of data. Figure 5 shows the obtained strain deformation pattern from the
273   experiment (a) and the simulation (b). The expected, homogenous strain pattern over the central
274   region of the membrane is evident from the results. Experiment and simulation agree well and
275   provide an average strain of 1.38±0.021% and 1.49%, respectively.
276   The results provide a better understanding of the membrane deformation and confirm the
277   homogenous strain pattern for the subsequent cell stretching experiments. Figure 5 clearly shows
278   that we could expect a homogenous strain pattern that in the central region of the membrane. Thus,
279   it can be assumed that cells located in this region will experience an equal amount of the strain.

280   *3.3 Cell area and aspect ratio*

281   Figure 6 shows the obtained averaged cell area and aspect ratio for each predefined time point.
282   The results show the gradual decrease in the cell area for cyclic stretching as a result of cell
283   displacement and aggregation. The cell aspect ratio for the over stretching duration for a maximum
284   of 4 hours also decreased which was in line with the previously reported observations.[39-42] The
285   morphological observation suggests that both cyclic and static stretching led to significant changes
286   in fibroblast adherence. However, we focused more on the cyclic stretching as native tissues within
287   the body are more exposed to a cyclic strain rather than static strain. Under cyclic strain,
288   mechanotransduction and intercellular physiology involving cytoskeletal elements and adhesion
289   molecules drive the morphogenetic process of cells.[43] The cells respond adaptively against
290   external stress transmission and reorganize their cytoskeleton integrity by reconstructing the actin
291   stress fibres. [44,45] We also observed that cyclic stretching of the fibroblast cell culture triggered
292   the formation stress fibres, and over time cells enhanced their cell-cell connection and formed cell
293   clusters.
294   The reorganization of actin stress fibres seems to promote cell adhesion dynamic and to change
295   cell morphology.[46] Furthermore, it was interesting to note that after two hours of cyclic stretching,
296   significant formation of cell clusters was observed. The stronger cell connections and the formation
297   of cell clusters explain how individual cell sense and transmit the physical forces to neighbouring
298   cell by binding of adhesion molecules to expand cell-cell cohesion.[47]
299
300   Furthermore, it is interesting to address the question why stretching induces cell rearrangement
301   and adhesion of the cells into clusters. Generally, cells on a substrate surface are dynamic in nature
302   and are constantly reorganizing their actin filament network to retract and extend protrusions (the
303   formation of lamellipodia and filopodia). At the cellular level, changes in the surface topology lead
304   to the underlying processes involved in the maintenance of mechanical homeostasis.[48] The stress
305   fibres are projecting tension-bearing bundles of actin filaments, which act as a non-muscle
306   sarcomeres .[49] Cyclic stretching seems to trigger actin fibres to realign and to establish stronger
307   adhesive cell-cell connections to resist the strain.[50] Thus, we hypothesise that actin organization
308   under stress is critical for promoting cell adhesion dynamics to form cell aggregates and to
309   withstand the applied strain.

310   In contrast, cell area and aspect ratio for the static stretching did not change significantly. The cells
311   did not spread and promoted the formation of actin stress fibres under static strain as compared
312   with cyclic strain, Fig. 6. Additionally, no significant cell clusters were observed in static strain
313   mode. This discrepancy further suggests that prolonged static stretching imposes different effect on
314   the regulation of ECM and adhesion proteins. Previous investigations of the effect of static strains
315   alone on ECM synthesis showed the degradation of ECM and adhesion molecules.[51] In a recent
316   study, Cui *et al*. showed that cytoskeleton organization differs for cyclic and static and indicated that
317   cyclic stretching promote actin fibre formation and cell spreading.[52]   Moreover, as expected for
318   non-stretching (control) condition, the actin stress fibres were randomly distributed and no
319   significant changes in cell area and aspect ratio was observed.

320
321
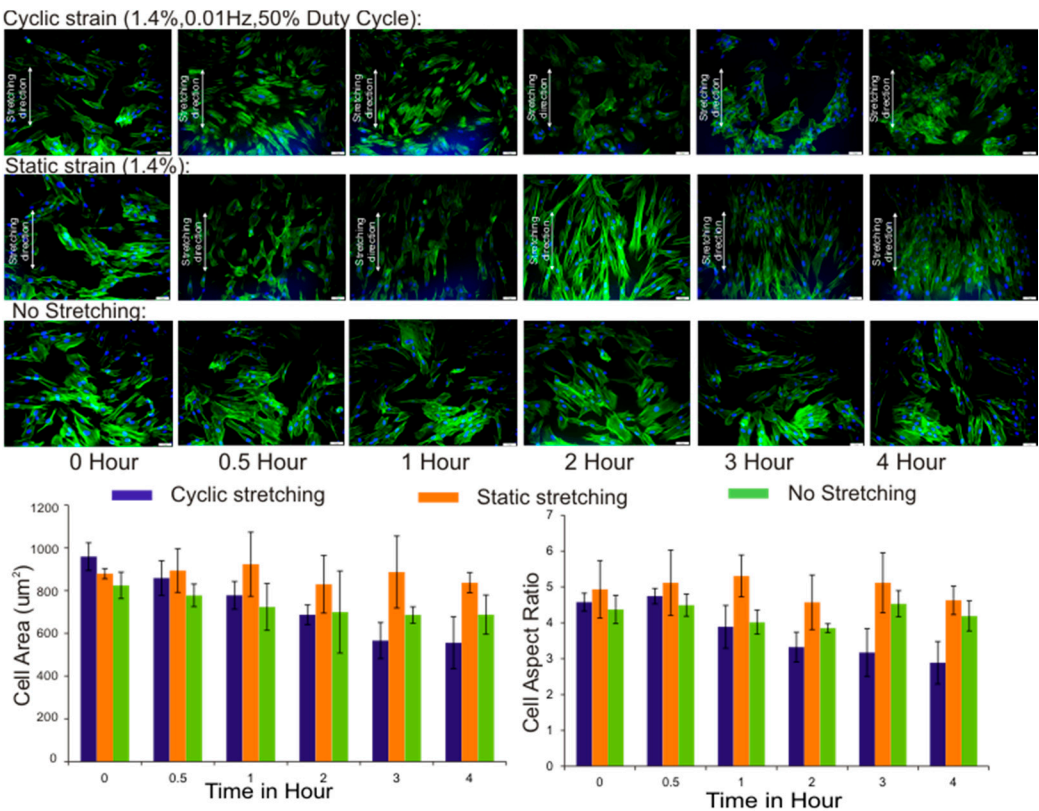322

323   *3.4 Cell orientation*

Fig. 6 Analysis results of cell area and aspect ratio for cyclic, static and no stretch conditions over the predefined time points (Inset: fluorescent images of the fibroblast cells with 20x objective for corresponding time points with 50-μm scale bar).

324   The orientation range of 0°-180^{0} was considered for the cell orientation analysis, which was
325   further divided into six equal angular regions in 30^{0} increments. For quantitative analysis of the cell
326   orientation, the 0° to 180° was set along the stretching direction in anti-clockwise direction and total
327   number of 900 samples from the three images of the ROI were analysed using ImageJ for each time
328   instance. Figure 7 shows the distribution of the cell orientation for each time instance. It was
329   interesting to observe distinct cell orientation trend for cyclic and static stretching modes. Under
330   cyclic stretching mode, the cell orientation showed two distinct peaks over 30-60^{0} and 120-150^{0}
331   range. The prominent cell orientation was observed after 1 hour of cyclic stretching. Whereas, under
332   the static stretching condition two distinct peaks were observed over 0-30^{0} and 150-180^{0} range.
333   Furthermore, it was interesting to observe that the prominence of the cell orientation under the static
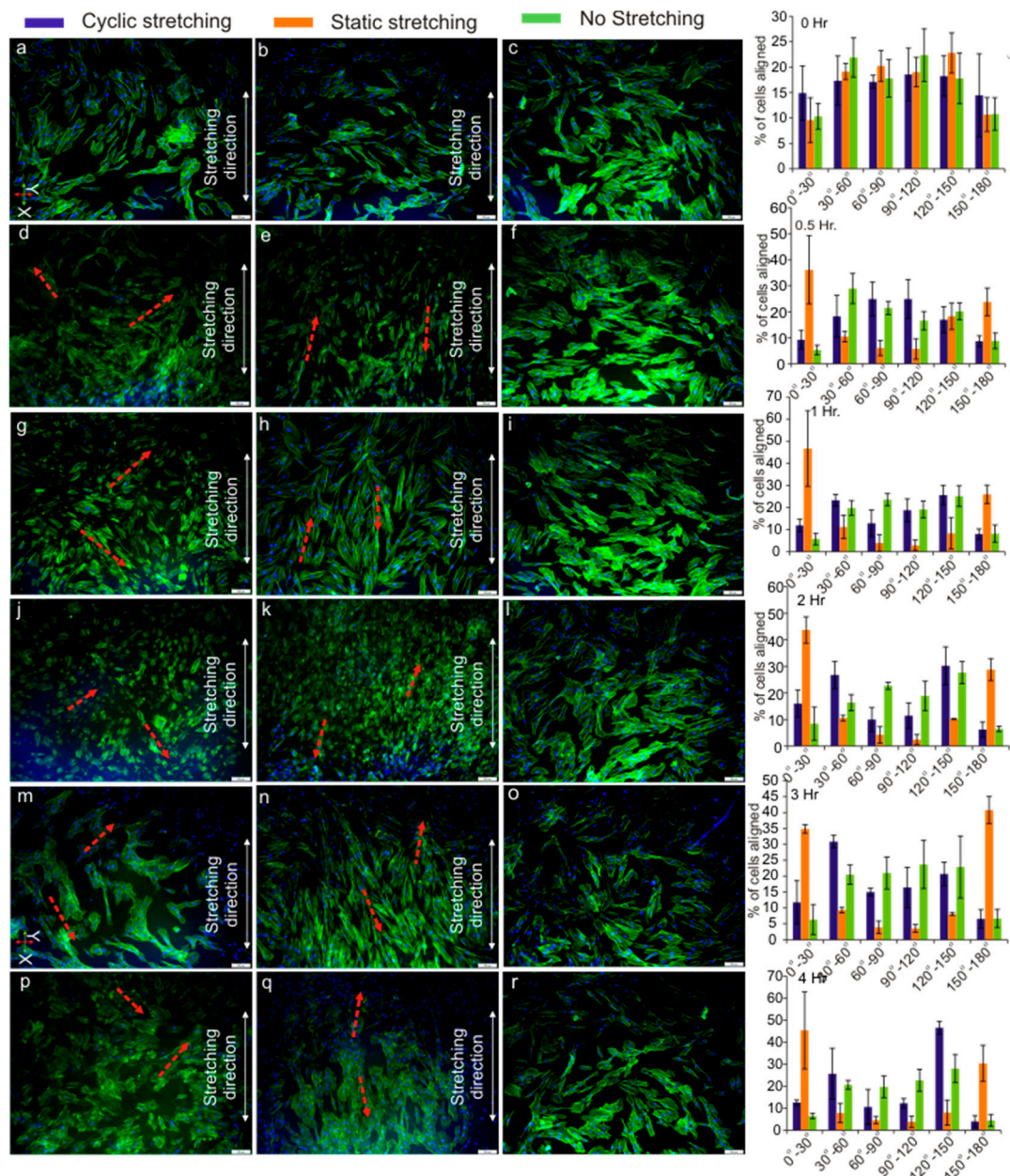

Fig. 7 Cell orientation analysis results for cyclic stretching (1.4%.0.01Hz,50% Duty Cycle) , static stretching (1.4%) and no stretching condition at 0 hr , 0.5 hrs ,1 hrs, 2 hrs , 3 hrs   and 4 hrs . (Inset: fluorescent images of the fibroblast cells with 10x objective for 0 hr (a-c), 0.5 hrs (d-f), 1 hrs (g-i), 2 hrs (j-l), 3 hrs (m-n) and 4 hrs (p-r) with 100-μm scale bar).

334 stretching conditions increased over the time. From this observation, we can conclude that most of
335 the cells are oriented approximately either at 45^0 or 135^0 under cyclic stretching and at 15^0 or 165^0
336 under static stretching condition (Fig.7 inset depicted by arrows).

337   Furthermore, as expected for the non-stretching condition, random distribution of the cell
338 orientation was observed. Two distinct and almost symmetric peaks were observed for both cyclic
339 and static stretching modes. This observation provides important evidence on the ability of the
340 fibroblast cells to recognize and respond not only to the applied strain but also to the strain
341 direction.[53-55] We found that fibroblasts reorient in an optimal angle to avoid the strain.
342 Moreover, actin stress fibres arrangement is clearly involved in the realignment of the cells under
343 strain. Our observation agrees with previous studies which reported that cells reorient and align
344 themselves due to external strain.[53,56-61]

345   The adhesion dynamic of cells are guided by cytoskeleton rearrangement and was believed to
346 be responsible for the cell alignment.[50,54] The cell–ECM connections are established by association
347 between actin stress fibres and the focal adhesion which endows cells to form stronger ECM
348 connections and cell-cell adhesion.[62,63] The focal adhesion is responsible for reorienting cells to a
349 direction where cells can maintain their stability. [54] In line with this hypothesis, we also observed a
350 cytoskeleton organisation and a distinct cell orientation under both cyclic and static stretching
351 conditions. In contrast, the non-stretching (control) conditions led to random distribution of the cell
352 orientation.

5. Conclusions

354   In summary, we developed a simple yet effective cell stretching platform capable of
355 introducing homogeneous cyclic and static strain onto the cell culture. The characterisation of the
356 developed platform provides a clear understanding of the device function. Furthermore,
357 effectiveness of the developed platform was tested with stretching assays of fibroblasts. Our
358 preliminary analysis suggested that the orientation of the cells is highly influenced by external
359 mechanical cues. The cell aggregation observed in the cyclic stretching mode suggests that the cells
360 reorganise their cytoskeleton to avoid external strain and to maintain intact extracellular matrix
361 arrangements. The developed cell stretching platform may serve as a tool to investigate the cell
362 behaviour for a wide range of strain with cyclic or static stretching conditions. Considering these
363 preliminary results, the platform may facilitate the active manipulation of the fibroblasts to achieve
364 the desired cell arrangements. This alternative cell culture method will have a broad range of
365 applications in the field of tissue remodelling and regenerative medicine. Furthermore, it is also
366 important to note that cells can be harvested after stretching using general clinical tools to perform
367 standard biology analysis which could be critical for clinical diagnosis and subsequent therapeutic
368 screening.

373 **Author Contributions:** H.K., N.T.N. and S.P. conceived and designed the experiments; H.K., R.V., M.B., K.B.
374 performed the experiments; H. K., M.J.A.S. and N.T.N. analyzed the data; H.K. and N.T.N. wrote the paper.

375 **Conflicts of Interest:** The authors declare no conflict of interest

References

377 1.   Chen, C.S. Mechanotransduction – a field pulling together? *J. Cell Sci.* **2008**, *121*,
378   3285.
379 2.   Silver, F.H.; Siperko, L.M. Mechanosensing and mechanochemical transduction:
380   How is mechanical energy sensed and converted into chemical energy in an
381   extracellular matrix? *Crit. Rev. Biomed. Eng.* **2003**, *31*, 255-331.

382 3.   Orr, A.W.; Helmke, B.P.; Blackman, B.R.; Schwartz, M.A. Mechanisms of
383   mechanotransduction. *Dev. Cell* **2006**, *10*, 11-20.
384 4.   Ingber, D.E. Mechanobiology and diseases of mechanotransduction. *Annals of*
385   *medicine* **2003**, *35*, 564-577.
386 5.   DuFort, C.C.; Paszek, M.J.; Weaver, V.M. Balancing forces: Architectural control of
387   mechanotransduction. *Nat. Rev. Mol. Cell Biol.* **2011**, *12*, 308-319.
388 6.   Mammoto, T.; Ingber, D.E. Mechanical control of tissue and organ development.
389   *Development* **2010**, *137*, 1407-1420.
390 7.   Klingberg, F.; Hinz, B.; White, E.S. The myofibroblast matrix: Implications for tissue
391   repair and fibrosis. *The Journal of pathology* **2013**, *229*, 298-309.
392 8.   Chiquet, M.; Renedo, A.S.; Huber, F.; Flück, M. How do fibroblasts translate
393   mechanical signals into changes in extracellular matrix production? *Matrix biology*
394   **2003**, *22*, 73-80.
395 9.   Schwartz, M.A. Integrins and extracellular matrix in mechanotransduction. *Cold*
396   *Spring Harb Perspect Biol* **2010**, *2*, a005066.
397 10. Fletcher, D.A.; Mullins, R.D. Cell mechanics and the cytoskeleton. *Nature* **2010**, *463*,
398   485-492.
399 11. Fletcher, D.A.; Mullins, R.D. Cell mechanics and the cytoskeleton. *Nature* **2010**, *463*,
400   485-492.
401 12. Hoon, J.L.; Tan, M.H.; Koh, C.G. The regulation of cellular responses to mechanical
402   cues by rho gtpases. *Cells* **2016**, *5*.
403 13. Wang, J.H.-C.; Yang, G.; Li, Z.; Shen, W. Fibroblast responses to cyclic mechanical
404   stretching depend on cell orientation to the stretching direction. *Journal of*
405   *Biomechanics* **2004**, *37*, 573-576.
406 14. De, R.; Zemel, A.; Safran, S.A. Dynamics of cell orientation. *Nature Physics* **2007**, *3*,
407   655-659.
408 15. Deguchi, S.; Kudo, S.; Matsui, T.S.; Huang, W.; Sato, M. Piezoelectric
409   actuator-based cell microstretch device with real-time imaging capability. *AIP*
410   *Advances* **2015**, *5*, 067110.
411 16. Tremblay, D.; Chagnon-Lessard, S.; Mirzaei, M.; Pelling, A.E.; Godin, M. A
412   microscale anisotropic biaxial cell stretching device for applications in
413   mechanobiology. *Biotechnol. Lett* **2014**, *36*, 657-665.
414 17. Kamble, H.; Barton, M.J.; Jun, M.; Park, S.; Nguyen, N.-T. Cell stretching devices as
415   research tools: Engineering and biological considerations. *LChip* **2016**, *16*,
416   3193-3203.
417 18. Esch, E.W.; Bahinski, A.; Huh, D. Organs-on-chips at the frontiers of drug discovery.
418   *Nat. Rev. Drug Discov.* **2015**, *14*, 248-260.
419 19. Nishimura, S.; Seo, K.; Nagasaki, M.; Hosoya, Y.; Yamashita, H.; Fujita, H.; Nagai,
420   R.; Sugiura, S. Responses of single-ventricular myocytes to dynamic axial stretching.
421   *Prog. Biophys. Mol. Biol.* **2008**, *97*, 282-297.
422 20. Chaudhuri, O.; Parekh, S.H.; Lam, W.A.; Fletcher, D.A. Combined atomic force
423   microscopy and side-view optical imaging for mechanical studies of cells. *Nat.*
424   *Methods* **2009**, *6*, 383-387.

425   21.   Sniadecki, N.J.; Lamb, C.M.; Liu, Y.; Chen, C.S.; Reich, D.H. Magnetic microposts
426   for mechanical stimulation of biological cells: Fabrication, characterization, and
427   analysis. *Rev. Sci. Instrum.* **2008**, *79*, 044302.
428   22.   Tan, Y.H.; Sun, D.; Wang, J.Z.; Huang, W.H. Mechanical characterization of human
429   red blood cells under different osmotic conditions by robotic manipulation with
430   optical tweezers. *IEEE Trans. Biomed. Eng.* **2010**, *57*, 1816-1825.
431   23.   Dhein, S.; Schreiber, A.; Steinbach, S.; Apel, D.; Salameh, A.; Schlegel, F.; Kostelka,
432   M.; Dohmen, P.M.; Mohr, F.W. Mechanical control of cell biology. Effects of cyclic
433   mechanical stretch on cardiomyocyte cellular organization. *Prog. Biophys. Mol. Biol.*
434   **2014**, *115*, 93-102.
435   24.   Higgins, S.; Lee, J.S.; Ha, L.; Lim, J.Y. Inducing neurite outgrowth by mechanical
436   cell stretch. *Biores Open Access.* **2013**, *2*, 212-216.
437   25.   He, Z.; Potter, R.; Li, X.; Flessner, M. Stretch of human mesothelial cells increases
438   cytokine expression. *Adv. Perit. Dial.* **2012**, *28*, 2-9.
439   26.   Nava, G.; Bragheri, F.; Yang, T.; Minzioni, P.; Osellame, R.; Cristiani, I.;
440   Berg-Sørensen, K. All-silica microfluidic optical stretcher with acoustophoretic
441   prefocusing. *Microfluid. Nanofluid.* **2015**, *19*, 837-844.
442   27.   Huang, Y.; Nguyen, N.T. A polymeric cell stretching device for real-time imaging
443   with optical microscopy. *Biomed. Microdevices* **2013**, *15*, 1043-1054.
444   28.   Tremblay, D.; Chagnon-Lessard, S.; Mirzaei, M.; Pelling, A.E.; Godin, M. A
445   microscale anisotropic biaxial cell stretching device for applications in
446   mechanobiology. *Biotechnol. Lett* **2014**, *36*, 657-665.
447   29.   Shao, Y.; Tan, X.; Novitski, R.; Muqaddam, M.; List, P.; Williamson, L.; Fu, J.; Liu,
448   A.P. Uniaxial cell stretching device for live-cell imaging of mechanosensitive
449   cellular functions. *Rev. Sci. Instrum.* **2013**, *84*, 114304.
450   30.   Shimizu, K.; Shunori, A.; Morimoto, K.; Hashida, M.; Konishi, S. Development of a
451   biochip with serially connected pneumatic balloons for cell-stretching culture.
452   *Sensors Actuators B: Chem.* **2011**, *156*, 486-493.
453   31.   Kamotani, Y.; Bersano-Begey, T.; Kato, N.; Tung, Y.C.; Huh, D.; Song, J.W.;
454   Takayama, S. Individually programmable cell stretching microwell arrays actuated
455   by a braille display. *Biomaterials* **2008**, *29*, 2646-2655.
456   32.   Huang, L.; Mathieu, P.S.; Helmke, B.P. A stretching device for high-resolution
457   live-cell imaging. *Ann. Biomed. Eng.* **2010**, *38*, 1728-1740.
458   33.   Sraj, I.; Eggleton, C.D.; Jimenez, R.; Hoover, E.; Squier, J.; Chichester, J.; Marr,
459   D.W.M. Cell deformation cytometry using diode-bar optical stretchers. *JBO* **2010**,
460   *15*, 047010.
461   34.   Scuor, N.; Gallina, P.; Panchawagh, H.V.; Mahajan, R.L.; Sbaizero, O.; Sergo, V.
462   Design of a novel mems platform for the biaxial stimulation of living cells. *Biomed.*
463   *Microdevices* **2006**, *8*, 239-246.
464   35.   Iwadate, Y.; Yumura, S. Cyclic stretch of the substratum using a shape-memory alloy
465   induces directional migration in dictyostelium cells. *Biotechniques* **2009**, *47*,
466   757-767.

36. Guido, I.; Xiong, C.; Jaeger, M.S.; Duschl, C. Microfluidic system for cell mechanics analysis through dielectrophoresis. *Microelectron. Eng.* **2012**, *97*, 379-382.

37. Kamble, H.; Barton, M.J.; Nguyen, N.-T. Modelling of an uniaxial single-sided magnetically actuated cell-stretching device. *Sensors and Actuators A: Physical* **2016**, *252*, 174-179.

38. Harshad, K.; Jun, M.; Park, S.; Barton, M.J.; Vadivelu, R.K.; St John, J.; Nguyen, N.T. An electromagnetic cell-stretching device for mechanotransduction studies of olfactory ensheathing cells. *Biomed Microdevices* **2016**, *18*, 45.

39. Mann, J.M.; Lam, R.H.; Weng, S.; Sun, Y.; Fu, J. A silicone-based stretchable micropost array membrane for monitoring live-cell subcellular cytoskeletal response. *Lab Chip* **2012**, *12*, 731-740.

40. Mao, X.; Said, R.; Louis, H.; Max, J.P.; Bourhim, M.; Challande, P.; Wahl, D.; Li, Z.; Regnault, V.; Lacolley, P. Cyclic stretch-induced thrombin generation by rat vascular smooth muscle cells is mediated by the integrin alphavbeta3 pathway. *Cardiovasc. Res.* **2012**, *96*, 513-523.

41. Sethi, K.; Cram, E.J.; Zaidel-Bar, R. Stretch-induced actomyosin contraction in epithelial tubes: Mechanotransduction pathways for tubular homeostasis. *Semin. Cell Dev. Biol.* **2017**.

42. Geiger, B.; Yamada, K.M. Molecular architecture and function of matrix adhesions. *Cold Spring Harb. Perspect. Biol.* **2011**, *3*, a005033.

43. Boccafoschi, F.; Bosetti, M.; Sandra, P.M.; Leigheb, M.; Cannas, M. Effects of mechanical stress on cell adhesion: A possible mechanism for morphological changes. *Cell Adh Migr* **2010**, *4*, 19-25.

44. Kassianidou, E.; Kumar, S. A biomechanical perspective on stress fiber structure and function. *Biochim Biophys Acta* **2015**, *1853*, 3065-3074.

45. Kaunas, R. Sarcomeric model of stretch-induced stress fiber reorganization. **2010**.

46. Ngu, H.; Feng, Y.; Lu, L.; Oswald, S.J.; Longmore, G.D.; Yin, F.C. Effect of focal adhesion proteins on endothelial cell adhesion, motility and orientation response to cyclic strain. *Ann Biomed Eng* **2010**, *38*, 208-222.

47. Bazellieres, E.; Conte, V.; Elosegui-Artola, A.; Serra-Picamal, X.; Bintanel-Morcillo, M.; Roca-Cusachs, P.; Munoz, J.J.; Sales-Pardo, M.; Guimera, R.; Trepat, X. Control of cell-cell forces and collective cell dynamics by the intercellular adhesome. *Nat Cell Biol* **2015**, *17*, 409-420.

48. Parsons, J.T.; Horwitz, A.R.; Schwartz, M.A. Cell adhesion: Integrating cytoskeletal dynamics and cellular tension. *Nat Rev Mol Cell Biol* **2010**, *11*, 633-643.

49. Verkhovsky, A.B.; Borisy, G.G. Non-sarcomeric mode of myosin ii organization in the fibroblast lamellum. *J Cell Biol* **1993**, *123*, 637-652.

50. Tondon, A.; Kaunas, R. The direction of stretch-induced cell and stress fiber orientation depends on collagen matrix stress. *PLoS One* **2014**, *9*, e89592.

51. Gupta, V.; Grande-Allen, K.J. Effects of static and cyclic loading in regulating extracellular matrix synthesis by cardiovascular cells. *Cardiovasc Res* **2006**, *72*, 375-383.

509 52.   Cui, Y.; Hameed, F.M.; Yang, B.; Lee, K.; Pan, C.Q.; Park, S.; Sheetz, M. Cyclic
510   stretching of soft substrates induces spreading and growth. *Nat. Commun.* **2015**, *6*,
511   6333.

512 53.   Pavesi, A.; Adriani, G.; Rasponi, M.; Zervantonakis, I.K.; Fiore, G.B.; Kamm, R.D.
513   Controlled electromechanical cell stimulation on-a-chip. *Sci. Rep.* **2015**, *5*, 11800.

514 54.   Wang, L.; Li, Y.; Chen, B.; Liu, S.; Li, M.; Zheng, L.; Wang, P.; Lu, T.J.; Xu, F.
515   Patterning cellular alignment through stretching hydrogels with programmable strain
516   gradients. *ACS applied materials & interfaces* **2015**, *7*, 15088-15097.

517 55.   Chagnon-Lessard, S.; Jean-Ruel, H.; Godin, M.; Pelling, A.E. Cellular orientation is
518   guided by strain gradients. *Integr Biol (Camb)* **2017**.

519 56.   Wang, J.H.; Yang, G.; Li, Z. Controlling cell responses to cyclic mechanical
520   stretching. *Ann. Biomed. Eng.* **2005**, *33*, 337-342.

521 57.   Wang, Q.; Huang, H.; Wei, K.; Zhao, Y. Time-dependent combinatory effects of
522   active mechanical loading and passive topographical cues on cell orientation.
523   *Biotechnol. Bioeng.* **2016**, *113*, 2191-2201.

524 58.   Weidenhamer, N.K.; Tranquillo, R.T. Influence of cyclic mechanical stretch and
525   tissue constraints on cellular and collagen alignment in fibroblast-derived cell sheets.
526   *Tissue engineering. Part C, Methods* **2013**, *19*, 386-395.

527 59.   Abiko, H.; Fujiwara, S.; Ohashi, K.; Hiatari, R.; Mashiko, T.; Sakamoto, N.; Sato,
528   M.; Mizuno, K. Rho guanine nucleotide exchange factors involved in cyclic-stretch-
529   induced reorientation of vascular endothelial cells. *J Cell Sci* **2015**, *128*, 1683-1695.

530 60.   Wang, J.H.; Yang, G.; Li, Z.; Shen, W. Fibroblast responses to cyclic mechanical
531   stretching depend on cell orientation to the stretching direction. *J Biomech* **2004**, *37*,
532   573-576.

533 61.   Papadopoulou, A.; Iliadi, A.; Eliades, T.; Kletsas, D. Early responses of human
534   periodontal ligament fibroblasts to cyclic and static mechanical stretching. *Eur. J.*
535   *Orthod.* **2016**, 258-263.

536 62.   Blanchoin, L.; Boujemaa-Paterski, R.; Sykes, C.; Plastino, J. Actin dynamics,
537   architecture, and mechanics in cell motility. *Physiol Rev* **2014**, *94*, 235-263.

538 63.   Burridge, K.; Guilluy, C. Focal adhesions, stress fibers and mechanical tension. *Exp*
539   *Cell Res* **2016**, *343*, 14-20.

540